PAPER

Check for updates

How ambient conditions affect the Leidenfrost temperature†

Michiel A. J. van Limbeek, ✶[ab] Olinka Ramírez-Soto, [ab] Andrea Prosperetti[ac] and Detlef Lohse ✶[ab]

By sufficiently heating a solid, a sessile drop can be prevented from contacting the surface by floating on its own vapour. While certain aspects of the dynamics of this so-called Leidenfrost effect are understood, it is still unclear why a minimum temperature (the Leidenfrost temperature T_L) is required before the effect manifests itself, what properties affect this temperature, and what physical principles govern it. Here we investigate the dependence of the Leidenfrost temperature on the ambient conditions: first, by increasing (decreasing) the ambient pressure, we find an increase (decrease) in T_L. We propose a rescaling of the temperature which allows us to collapse the curves for various organic liquids and water onto a single master curve, which yields a powerful tool to predict T_L. Secondly, increasing the ambient temperature stabilizes meta-stable, levitating drops at increasingly lower temperatures below T_L. This observation reveals the importance of thermal Marangoni flow in describing the Leidenfrost effect accurately. Our results shed new light on the mechanisms playing a role in the Leidenfrost effect and may help to eventually predict the Leidenfrost temperature and achieve complete understanding of the phenomenon, however, many questions still remain open.

1 Introduction

When a drop is deposited on a hot surface, a vapour film is formed, provided that the temperature of the surface exceeds the so-called Leidenfrost temperature.[1] In this situation, the contact between the liquid and the hot surface is prevented by the vapour film. This effect manifests itself during spray combustion,[2] liquid spreading[3] and is very undesirable in contexts where evaporation is employed for temperature control, such as spray cooling.[4] The insulating vapour layer between the liquid and the solid prevents efficient heat transfer. Therefore the Leidenfrost effect has attracted a lot of attention, focussing on the shape and the vapour layer thickness of the drops[5–7] and the influence of the impact dynamics.[4,8–12] The minimal temperature of the solid required for the effect to manifest itself is called the Leidenfrost temperature T_L (after the first systematic description of the phenomen by Johann Gottlob Leidenfrost,[13] although in fact it

had first been mentioned already by Herman Boerhaave[14] two decades earlier). The Leidenfrost temperature is often determined by observing when the drop has a 180° contact angle[5,8,13] or a (local) maximum in its lifetime.[6]

Once a drop is in the Leidenfrost state, for the vapour film thickness and profile, good agreement between observations and modelling is achieved.[5,15] The typical thickness h of the vapour layer scales with the superheat $\Delta T = (T - T_{sat})$ as $h \propto \Delta T^{1/4}$, where T is the plate temperature and T_{sat} the saturation (*i.e.*, boiling) temperature.[5–7] However, the models predicting such scaling do not hold for vanishing superheat: no stable Leidenfrost drops are documented in literature for a plate temperature $T \to T_{sat}$, whereas the models still predict a vapour layer in this limit *e.g.* in the order of micrometers for a superheat of $\Delta T = 1$ K, much thicker than any long range forces. A few observations of unstable Leidenfrost drops exist however. Drops on superheated liquid pools[16–18] and drops which are on a hot plate which was initially above T_L, but which is cooling down over time below T_L[5,19] while the drop remains in the Leidenfrost state. Once the vapour film of these unstable drops gets pierced however, they do not recover back to the Leidenfrost state. Recently, this regime was explored by utilizing superhydrophobic surfaces to prevent wetting.[20] In contrast to the classical boiling curve for wetting drops, where a local maximum in the evaporation time is found at $T = T_L$, here, a monotonic decrease in evaporation time was observed with increasing plate temperature.

[a] *University of Twente, Physics of Fluids, Drienerlolaan 5, P. O. Box 217, 7500AE Enschede, The Netherlands. E-mail: m.a.j.vanlimbeek@utwente.nl, d.lohse@utwente.nl*

[b] *Max Planck Institute for Dynamics and Self-Organization, Am Faßberg 17, 37077 Göttingen, Germany*

[c] *University of Houston, Department of Mechanical Engineering, N207 Engineering Building 1, 4726 Calhoun Road, Houston (TX), USA*

† Electronic supplementary information (ESI) available: Figure of the Leidenfrost temperature as a function of the saturation temperature, both normalized by the critical temperature. See DOI: 10.1039/d0sm01570a

The prediction of the Leidenfrost temperature T_L is however still an unsolved problem. It is known that T_L depends on the type of liquid[21] as well as the roughness[22,23] and thermal conductivity[21,24–27] of the plate. We also know that it increases with increasing impact velocity of the drop.[4,8–11] Here we want to study how T_L depends on the ambient pressure and the ambient temperature, for otherwise fixed parameters. A recent study[28] found T_L of water and organic liquids[29,30] to decrease for reduced ambient pressures, but a more general approach for several liquids is still lacking in literature. We therefore will study various liquids under reduced and elevated pressures.

We divide the paper in two sections: after discussing the experimental aspects and general phenomenology (Sections 2 and 3), first (Section 4) we focus on the effect of the ambient pressure P on the Leidenfrost temperature. We will find a strong dependence of T_L on P and after rescaling provide a data collapse of this behaviour for various liquids on one master curve. Second (Section 5), we will study the influence of the ambient temperature T_0 on T_L. We will find the existence of meta-stable Leidenfrost drops for smaller superheats when increasing the ambient temperature T_0. We identify such metastable drops by the irreversibility towards the Leidenfrost state after disturbing them by vibration. In contrast, 'stable' Leidenfrost do recover back to their initial configuration after disturbances forced a touch-down onto the hot plate. The two sets of experiments provide new insight on the mechanism behind T_L, which is of great importance for understanding and predicting the Leidenfrost effect.

2 Experimental aspects

The general setup to study the Leidenfrost effect consists of a heated plate, a drop dispenser, a light source and a (high speed) camera, see Fig. 1. To avoid the influence of roughness and cooling effects in the solid, we use a silicon plate (ThorLabs WG81050), which is optically smooth and has good thermal conductivity and sufficient thickness of 5 mm to avoid any cooling effects.[21,25,27] The plate is resting on a brass heater

Fig. 1 Schematic of the setups used. Three variations were built, see the main text; two for varying the ambient pressure P, one to vary the ambient temperature T_{box}.

block, whose temperature is controlled by a PID controller. The surface temperature T of the silicon plate was measured prior to the experiment by a Pt-100 sensor to calibrate the set point of the controller. The plate was placed inside either one of three containers which were designed to (1) reduce or, (2) elevate the ambient pressure, and (3) to control the ambient temperature to T_{box}. The surrounding pressure is indicated by P, with an uncertainty of 0.01 bar for setup one and 2.05 bar for the second one. Fresh (dry) air entered the setup through a needle valve, which, together with the pump set the pressure. The second container was made of titanium, the inner wall of which served as the heated plate (i.e. without the silicon plate). The poor thermal conductivity of titanium needs to be taken into account.[21] Here, the pressure was set by a check valve and vapour was removed by a condenser. All containers had windows to observe the phenomenon. For visualization we used shadowgraphy recorded by a camera at 1000 fps to capture fast dynamics.

Drops were generated at the tip of a needle using a syringe pump (Harvard PHD2000) or a HPLC pump (Shimadzu), which was a few millimeter away from the heated surface to avoid any impact dynamics when the drops are generated. The drop size was constant for all pressures, but dependent on the type of liquid, scaling as $(\gamma d)^{1/3}$, where γ is the temperature dependent drop size and d the needle diameter. In the case of the third setup, a glass capillary instead of a needle was placed inside the drops to allow for constant feeding of the drop during the experiment. The balance between evaporation and feeding leads to a static situation, since the size of the drop was controlled by the feeding rate. Both methods resulted in drops larger than the capillary length, for which the drop size does not affect the dynamics greatly,[7] but below the regime where the puddles (i.e. large drops) exhibit shape oscillations.[31]

3 Phenomenology

When a cold drop approaches the heated plate during deposition, contact is prevented by the viscous pressure build up. In the absence of any evaporation, this is the classical phenomenon of a draining film. Here however, the hot plate heats the bottom of the drop, which starts to evaporate. The vapour generation replenishes the escaping air at early times, until the film contains only vapour. Dissolved gas in the liquid was found to contribute little in terms of gas flux.[32] When the evaporation is insufficient, the film breaks and the drop wets the surface, trapping small bubbles in the process. In Fig. 2 we show snapshots of ethanol drops for various plate temperatures T. For low plate superheats, the drop touches the plate after dispensing it from a needle and evaporates from the top. With increasing T, the bubbles start to grow faster and detach from the surface. The bubbles burst, causing great disturbances in the drop and finally fragmentation. The temperature range of this transitional behaviour is typically a few Kelvin. Beyond T_L, light can pass underneath the drop, which is observed as a bright stripe in Fig. 2. This indicates that the drop levitates above the plate on its own vapour layer and we use this
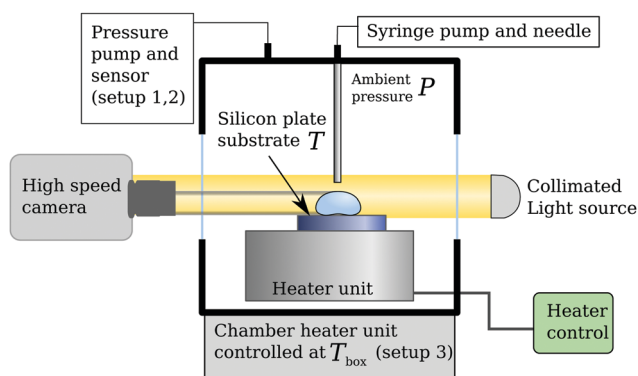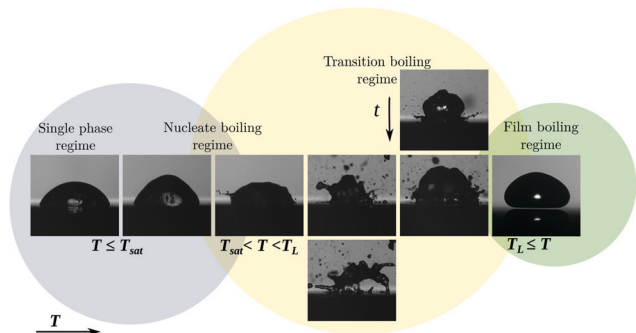
Fig. 2 Snapshots of liquid drops placed on a hot surface at different temperatures. Vertical placed snapshots slightly differ in time ($\Delta T \approx 1$ ms) to highlight the violent behaviour of the drop. The three coloured circles show the different main regimes.

throughout the study to identify the Leidenfrost state. The Leidenfrost phenomenon can occur for $T < T_L$ (the aforementioned metastable Leidenfrost drops) as well, where the gas/vapour film does not rupture when the dispensed drop approaches the hot plate and the evaporating drop balances the film draining process.

The vapour layer insulates the Leidenfrost drop, which results in a lower global evaporation rate[6] and lower heat transfer coefficient. The temperature of the liquid–vapour interface under the drop is fixed at the saturation temperature, which is determined by the ambient pressure of the setup. Initially, the bulk is not yet heated to saturation temperature and so is the top surface of the drop. As the surface tension depends on the temperature, the difference between the top and bottom temperature results in a stress imbalance on the interface. This Marangoni stress induces a flow in the bulk, transporting hot liquid away from the plate towards the top of the drop, see Fig. 9. Cold liquid descends in the centre, draining

additional heat from the plate. Since the top of the drop is now at an elevated temperature, additional evaporation takes place, for which the latent heat is removed from the drop. In contrast to the vapour film below the drop, which contains pure vapour, here, evaporation takes place into dry air. Two boundary layers form around the drop: a thermal layer which limits additional convective heat transfer to the surroundings, and a mass boundary layer, controlling the evaporation rate. The magnitudes of the fluxes are thus controlled by the (far-field ambient) temperature, since the vapour concentration depends on it. In the present study however, the surroundings are flushed with dry air. We thus identified a complex interplay between the hot plate, the cold drop and environmental conditions, especially in the transient phase during the approach of the drop towards the plate. Energy from the plate is removed for heating the drop, evaporating liquid and heating the gas surrounding the plate. In our study, we focus on the dependence of T_L on the ambient pressure and temperature and their impact on metastable Leidenfrost drops.

4 Influence of surrounding pressure

The first set of experiments involves the reduction of the ambient pressure P below 1 bar down to 30 mbar, for which we studied six different liquids. While varying the pressure, we changed the set-point of the plate temperature and registered at which minimum plate temperature the drops were in a stable Leidenfrost configuration. The employed liquids were: water, n-heptane 2-propanol, ethanol, acetone (propanone) and FC-72 (perfluorohexane C6F14). The measured Leidenfrost temperatures are presented together with the (pressure dependent) saturation temperature $T_{sat}(P)$ in Fig. 3. The latter is equated using the Clausius–Clapeyron equation $T\dfrac{\mathrm{d}P}{\mathrm{d}T} = L\Delta v$, where L is the latent heat and Δv the volumetric change of the substance.
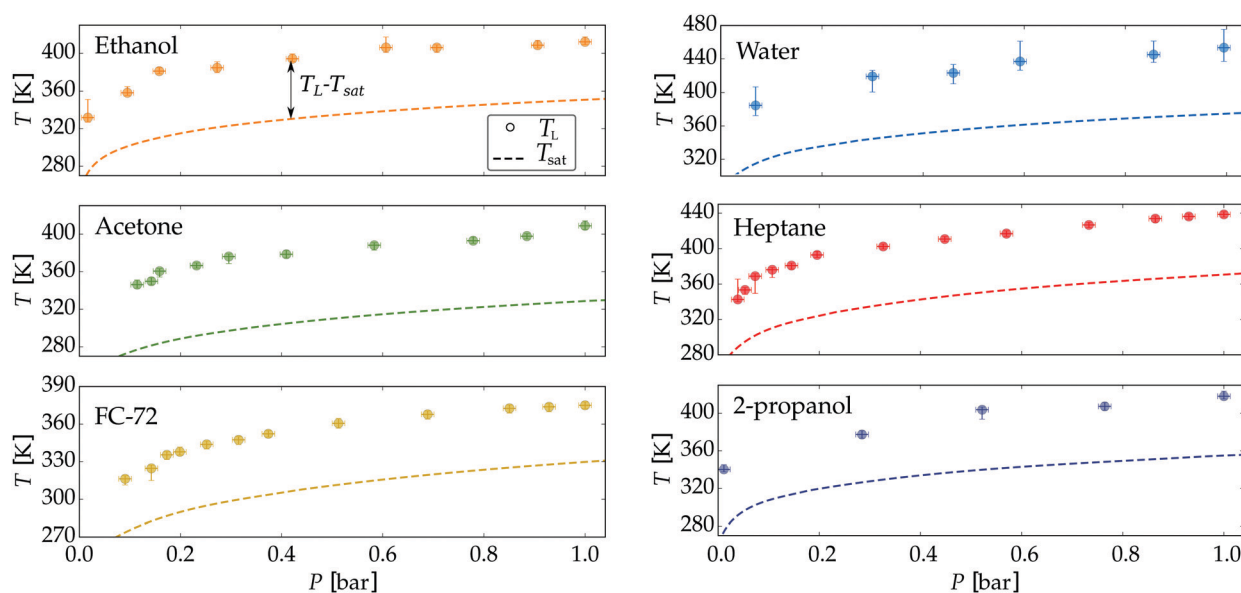

Fig. 3 Measured Leidenfrost temperature for six different liquids drops under reduced ambient pressure. The saturation temperature (dashed line) is calculated from the Clausius–Clapeyron equation using the coefficients from the NIST database.[38]

The datapoints indicate the minimal plate temperature where the drop does not touch the plate after dispensing. The bottom uncertainty is the minimal temperature at which a drop recovers from a sessile state into a Leidenfrost state, whereas the top uncertainty indicates the minimal plate temperature at which the drop never touches the plate during its evaporation. Note that these uncertainties in principle can coincide with the datapoint.

It is clear that for all liquids T_L shows a strong dependence on P. When plotting the Leidenfrost temperature against the saturation temperature, a linear trend appears for each liquid, with prefactors between 0.95 and 1.12, see Fig. 10. Since the film thickness scales with the superheat[5] $(T_L - T_{sat})^{1/4}$ no explicit dependency on P can be expected. For selfpropulsion[33–35] however, the force on the drop is affected by the vapour viscosity, which depends (non-trivially) on both the pressure and temperautre of the gas. Our results are in good agreement with those found by Mills and Fry[36] and Mills and Sharrock,[37] who studied T_L of alkanes and alcohols respectively at $P = 1$ bar. A linear relation between T_L and T_{sat} was found there, where the latter increases with increasing chain length of the alkanes resp. alcohols.

Since a linear dependence of the Leidenfrost temperature on the saturation temperature was found for all employed liquids, we now seek a unifying description, *i.e.* a single relation which holds for all liquids. The slopes b_1 of the fits

$$T_L = b_1 T_{sat} + b_0 \qquad (1)$$

seem to be independent of the employed liquids: although some variation in the exact value of b_1 was found, a single value would be within the error bounds of all liquids tested. In thermodynamic theory, liquid–vapour phase equilibria of various substances are successfully unified by rescaling the system parameters in terms of the critical temperature and pressure of the substance. It is tempting to employ this method here as well and rescale the experimental fit for T_L using the critical temperature T_c of the liquid to find a universal offset b_0. This however did not yield the desired collapse of the data (see Section 6, ESI†), from which we conclude that the manifestation of the Leidenfrost temperature is not a thermodynamical effect. Though liquid-dependent, the result indicates that the amount of superheat is important in the dewetting of the liquid from the plate, as observed during the experiment (see Fig. 2).

The employed liquids differ greatly in latent heat of evaporation L and gas specific heat $C_{p,g}$. The ratio between these two quantities appears naturally when solving the heat equation for the surrounding gas/vapour phase, see for instance.[39] The ratio $L/C_{p,g}$ can be interpreted as the relative amount of energy available for evaporation, compared to that being lost from the drop to the surrounding gas. We therefore define the non-dimensional temperature:

$$\Theta = T C_{p,g}/L \qquad (2)$$

and rescale the data presented in Fig. 4 accordingly, see Fig. 5. Note that $C_{p,g}/L$ is temperature dependent and was evaluated at $T_{sat}(P)$. For FC-72 and 2-propanol no data was available for L and $C_{p,g}$ and these cases are therefore not presented.
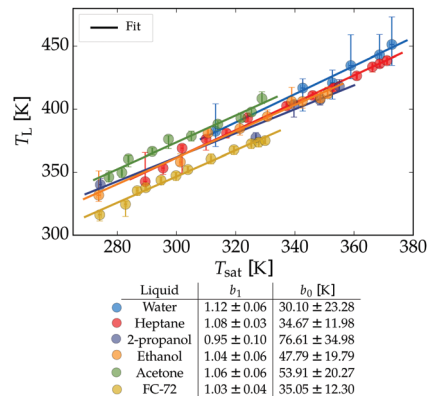

Fig. 4 The Leidenfrost temperature as a function of $T_{sat}(P)$, using the data of Fig. 3. The data is fitted by a linear relation: $T_L = b_1 \cdot T_{sat} + b_0$, where the coefficients are listed in the table.

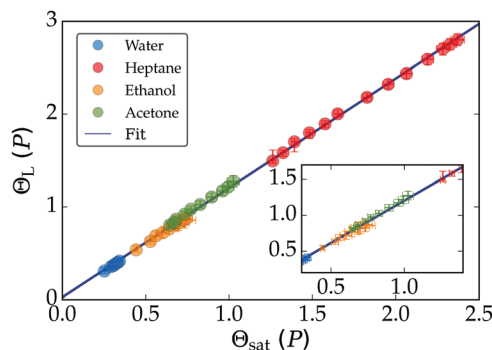| Liquid	b_1	b_0 [K]
Water	1.12 ± 0.06	30.10 ± 23.28
Heptane	1.08 ± 0.03	34.67 ± 11.98
2-propanol	0.95 ± 0.10	76.61 ± 34.98
Ethanol	1.04 ± 0.06	47.79 ± 19.79
Acetone	1.06 ± 0.06	53.91 ± 20.27
FC-72	1.03 ± 0.04	35.05 ± 12.30

Fig. 5 The linear relation between the non-dimensional saturation- and Leidenfrost temperatures of four liquids measured at reduced pressure. The data is fitted as $\Theta_L = 1.17 \Theta_{sat} + 0.02$. The inset is a zoom for small $\Theta_{sat}(P)$.

Fig. 6 shows additional data for various liquids which were only measured at 1 atmosphere. The measurements of T_L for various liquids at $P = 1$ show a linear relationship after rescaling
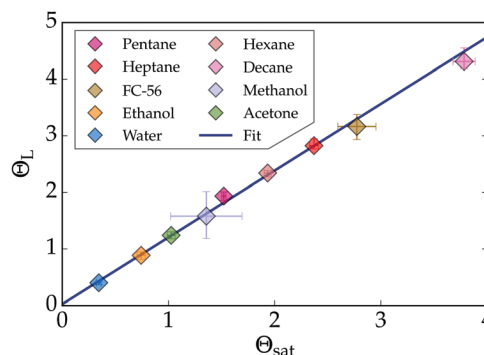

Fig. 6 The linear relation between the non-dimensional saturation- and Leidenfrost temperatures of various liquids measured ambient pressure ($P = 1$ bar). The data is fitted as $\Theta_L = 1.13 \Theta_{sat} + 0.08$. For comparison, some data from Fig. 4 was added.
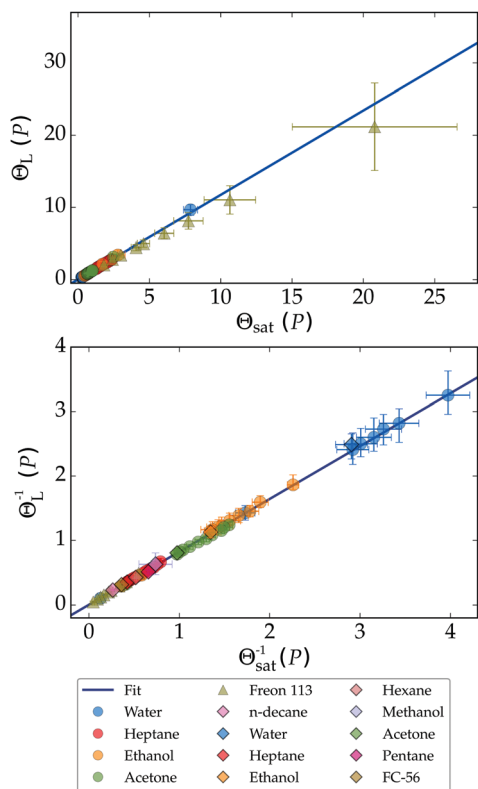
Fig. 7 All data for the non-dimensional Leidenfrost temperature can be collapsed onto a single curve (upper), described by $\Theta_L = 1.17\Theta_{sat} + 0.02$. The lower figure shows eqn (3), fitted as $\Theta_L^{-1} = 0.82\Theta_{sat}^{-1} + 0.004$.

as well, as can be seen in Fig. 6. Using the proposed rescaling we obtain a collapse of the data, with only two parameters for all employed liquids.

Using the second setup described in Section 2 we studied the Leidenfrost phenomena at elevated pressures for water, ethanol, and acetone. Data from ref. 30 for Freon 113 (1,1,2-trichloro-1,2,2-trifluoroethane) was added to test the rescaling towards the critical point. From the result of Fig. 7 we conclude that the found linear relation between the saturation and Leidenfrost temperature well predicts the latter for most liquids. The Freon data however start to deviate towards the critical temperature. We employ a second correlation to account for the observed non-linearity, which is of a similar form as the model suggested by Orejon et al.:[28]

$$\Theta_L^{-1} = a\Theta_{sat}^{-1} + \beta. \tag{3}$$

The result is presented in the lower panel of Fig. 7. Our data was fitted best for $a = 0.004$ and $\beta = 0.82$, which yielded after further manipulation the following universal relation for all experiments:

$$T_L = \frac{T_{sat}}{0.82 + 0.004 \dfrac{C_{p,g}}{L} T_{sat}}. \tag{4}$$

This nonlinear model can be expanded around any temperature T_0 linearly to recover eqn (1), where the coefficients depend

on T_0. It is clear that the non-linearity in $T_L(T_{sat})$, i.e. the correction term in the denominator, is important for large $C_{p,g}/L$ or T_{sat}. Since $C_{p,g}/L$ increases for $T_{sat}(P) \to T_c$ as well (T_c being the critical temperature), one can expect the non-linearity to manifest itself for increasing ambient pressure P. Close to T_c the ratio diverges as $L \to 0$, which however does not reduce eqn (4) to $T_L = T_{sat}$. Our data does not allow further speculation on the exact form in this limit.

5 Influence of the surrounding temperature: metastable Leidenfrost drops

5.1 Observations

Since we expect some heat losses to the surroundings (for instance from the top of the drop) we investigate the Leidenfrost temperature of ethanol while we vary the temperature T_{box} of the surrounding box. We reduced the complexity of the study by restricting us to a single liquid. The slow infusion rate of the syringe pump made forming drops first creep up the capillary, until the size became large enough to be pulled down by gravity, descending slowly towards the hot plate. Then, the drop could either directly wet the plate or be in a Leidenfrost state. The observations are presented in Fig. 8, where T_{min} denotes the lowest plate temperature where drops do not directly wet the plate, but enter the Leidenfrost state.

Next, every Leidenfrost drop was vibrated by touching the glass capillary. The drops then made contact with the plate, followed by one of two phenomena: (i) for moderate plate temperatures, the drops remained in contact with the plate, boiling violently, as presented by the transition boiling regime of Fig. 2, and rapidly boiled away. (ii) For higher plate temperature T, this behaviour changes and the drop recovers into the Leidenfrost state. The two scenarios are indicated by the snapshots of Fig. 8, where the arrow(s) indicate (ir)reversibility. Drops in scenario (i) are thus metastable, indicated by the gray area. Cleaning the silicon plate of residue from previously wetted drops and dust particles lowered T_{min} significantly, by several tens of
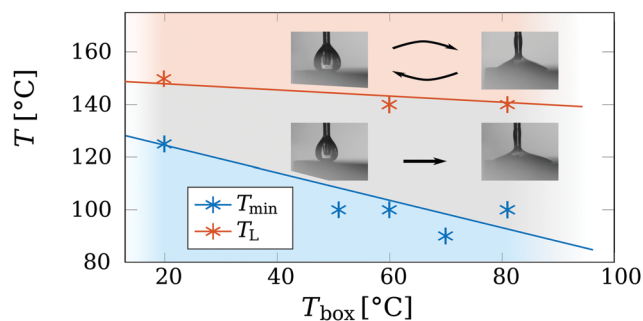

Fig. 8 Drops in a Leidenfrost state for varying T_{box}. The blue datapoints indicate the lowest plate temperature T_{min} where drops can survive in a Leidenfrost state (gray area). These drops are metastable drops as external influences disrupt the configuration resulting in a permanent touch-down of the drop. Plate temperatures above the red data points (red area) make drops always recover back to the Leidenfrost state after contacting the plate (lines are guides to the eye).

Kelvin. The cases where the drop did recover into the Leidenfrost state (scenario ii) are thus stable. The minimal plate temperature at which this reversible behaviour is observed is roughly 145 °C (red data points). This value agrees well within the literature values of 140 °C < T_L < 155 °C.[21,37] The amount of disturbance is not of great importance, as the aim of this study is not to quantify the robustness of metastable Leidenfrost drops against disturbances. Since this is a metastable system, such a study would also require control over the plate roughness and contamination levels of both the air, liquid and injection system, which is beyond the scope of this study. We here identified a third classification method of the Leidenfrost state, based on the ability of recovering from a wetted state. This method deals with the possibility of meta-stable drops, a distinction which the life time[6] of the drop or the 180° contact angle appearance cannot[5,8] provide.

To our knowledge, metastable Leidenfrost drops have only been reported as such only twice in literature.[5,19] In both studies, a water drop was placed on a hot surface above T_L. Then the heating was ceased and the plate temperature was lowered by a cooling circuit. Surprisingly, the Leidenfrost drop remained in this state at $T \approx 100$ °C. Contamination,[40] roughness and drop oscillations were suggested to be able to pierce the thinning vapour layer,[41] breaking the metastable configuration and making the drop wet the plate. Metastable drops are also found in the case of Leidenfrost drops on a pool, called a 'boule', which can survive on a superheat of a few Kelvin above saturation as well.[16,17] Contamination,[16] was identified for this system to control the stability of the vapour layer, highlighting the metastability of the 'boule'. Finally, small drops can be levitated by a Stefan flow even at conditions below the saturation temperature.[42]

We therefore concluded that, although Leidenfrost-like drops can be made at temperatures below T_L, these drops are metastable and can easily be forced into the contact-/nucleate-boiling state. The Leidenfrost state is therefore to be associated to a rapid change in contact line dynamics for which a drop starts to dewet the plate once contact has been made. Such a dramatic change can be observed by using high-speed FTIR-imaging. The gradual, diffusive bubble growth found for $T < T_L$ changes into rapid dewetting contact lines, where bubbles loose the spherical shape, see the movies of Shirota *et al.*[10] We thus propose that for the prediction of the (stable) Leidenfrost temperature, one needs to focus on the contact line dynamics and on how these are affected by an increasing superheat.

A trend can be observed for the minimum plate temperature T_{min} at which metastable drops can survive. As shown in Fig. 8, T_{min} approaches T_{sat} = 78 °C for ethanol with increasing T_{box}. This can readily be understood by introducing a vanishing effect of the Marangoni flow on the drop surface. The evaporation from the top of the drop makes the drop interface to cool locally.[43,44] As a result of the increase in surface tension by the local cooling, a surface tension gradient $\partial_r \Gamma$ occurs, scaling as $\partial_r \Gamma \approx \partial_T \Gamma \Delta T_{bt}/R$. Here Γ is the surface tension, ∂_T the partial derivative with respect to temperature and ΔT_{bt} the temperature difference between the top and bottom of the drop. The surface tension gradient induces a shear flow condition at the interface of the drop, including at the lower gap between the liquid and the vapour phase. The shear flow condition lowers the pressure build-up in the gap, resulting in a thinner gap thickness h. Thus, suppressing the Marangoni flow, by increasing the ambient temperature T_{box}, requires a lower plate temperature T to provide the same gap thickness. Next, we will formalize and quantify this argument by developing a simple model below to further evaluate this hypothesis.

5.2 Modelling

As discussed above, the heat losses from the top of the drop induce a temperature gradient. This leads to a Marangoni flow, inducing a shear stress condition on the drop interface. The shear stress is balanced by the viscous shear in both the vapour gap as well as the drop. The resulting velocity hence becomes a combination of a Couette and a Poiseuille flow, in which only the latter is balancing the pressure build-up under the drop to levitate the drop. Fig. 9 shows this model, which is formalized as follows: the solution for the gap thickness h must consider the Marangoni stress at the drop interface. Levitation requires the vertical pressure balance between the weight of the drop, $\rho g \mathscr{L}$ and the viscous pressure build-up in the gap. Below the capillary length $\ell_c = (\Gamma/(\rho_l g))^{1/2}$, we take the (horizontal) radius R as the vertical length scale, $\mathscr{L}$, whereas it saturates at $2\ell_c$ for puddles $R > \ell_c$. The separation of length-scales in the vapour gap allows for the use of the axi-symmetric steady Stokes equation, where $0 < y < h \ll R$.

$$\partial_r P = \eta_v \partial_{yy} u, \tag{5}$$

valid away from the symmetry axis (*i.e.* $r > h$). Here η is the viscosity, and u the (radial) vapour velocity. Subscripts v and l are used for the vapour and liquid phase, respectively. We then describe the flow in the vapour layer as a combination of a Poiseuille and Couette flow:

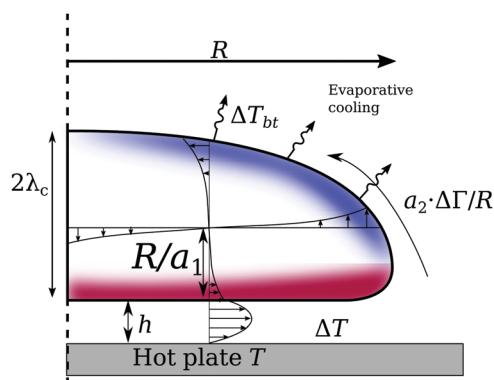$$u = U_p \frac{y}{h}\left(1 - \frac{y}{h}\right) + U_c \frac{y}{h}. \tag{6}$$

Fig. 9 Sketch of an (axi-symmetric) Leidenfrost drop, which is subject to evaporation on the top. The resulting Marangoni stress induces a shear flow in the gap, yielding a reduction in the gap thickness h and the emergence of a recirculation roll in the drop of radius R/a_1.

The Couette flow does not directly contribute to the levitation and is determined by the stress balance at the vapour–drop interface, including a Marangoni shear stress. The average flux then is:

$$\bar{u} = \frac{1}{h}\int_0^h u\,\mathrm{d}y = \frac{U_p}{6} + \frac{U_c}{2}, \qquad (7)$$

yielding

$$U_p = -\frac{h^2 \partial_r P}{2\eta_v}. \qquad (8)$$

The flow if driven by the over-pressure in the gap with respect to the ambient pressure, which was estimated before as $\rho g \ell_c$. The pressure would then drop over the radial length scale R, yielding a pressure gradient $\partial_r P = -\rho g \ell_c / R$. Using mass conservation, we find

$$\rho_v \partial_r (rh\bar{u}) = r\dot{m}(h), \qquad (9)$$

where $\dot{m}(h)$ is the mass generation. After rearranging and using Fourier's law, we find $\dot{m}/\rho_v = \varepsilon/h$, in which $\varepsilon = k_v \Delta T/(L\rho_v)$ groups the relevant thermo-physical parameters of the problem. After averaging over the gap thickness, this equation can be integrated across the gap length to obtain

$$h\left(\frac{U_p}{6} + \frac{U_c}{2}\right) = \frac{R}{2}\frac{\varepsilon}{h}. \qquad (10)$$

For the limiting case $U_c \to 0$, i.e. no slip, the model recovers that of Wachters[5] and Biance.[6]

The problem is closed by finding the velocity at the drop interface, U_c. This is set by satisfying the shear stress continuity: $\eta_l \partial_y u_l + \eta_v \partial_y u_v = \partial_r \Gamma$ for $y = h$.[45] We find $\partial_y u_v = (U_c - U_p)/h$. After some transient effects, recirculation emerges inside the drop. We allow for a large recirculation roll inside the drop, finding $\partial_y u_l \approx a_1 U_c/R$, where a_1 is a geometrical constant. For small drops, only a single cell exists,[44] for which $a_1 \approx 1$. For larger drops ($R \approx \ell_c$), a secondary cell emerges. Naturally, a_1 increases as well, thus we vary a_1 to study its role.

The Marangoni stress is modelled as $a_2 \Delta \Gamma/\mathscr{L} = a_2 \Delta T_{bt} \partial_T \Gamma/R$. This gradient varies over the length scale of the drop as well,

thus a_2 is also of order one. Bouillant et al.[44] studied the thermal gradient along the drop interface, from which we can use for $R < \ell_c$: $\Delta T_{bt} \approx 20$ K and $a_2 \approx 2$. For large drops however, $\Delta T_{bt} \approx 10$ K, but the gradient is localized close to the plate, leading to $a_2 \approx 5$. A more global estimate leads to $\Delta T_{bt} \approx 15$ and $a_2 = 1$. For all cases however, Bouillant et al.'s[44] observations yield for $a_2 \Delta T_{bt}$ a value between 20 K and 50 K.

We now solve eqn (10), where U_p and U_c are given by eqn (8) and the shear stress balance:

$$\eta_v \frac{U_c - U_p}{h} + a_1 \eta_l \frac{U_c}{R} = a_2 \frac{\Delta T_{bt} \partial_T \Gamma}{R}. \qquad (11)$$

The solutions without Marangoni stresses ($a_2 = 0$) are presented in Fig. 10 to highlight the role of the viscous stresses in the drop. The length scale R/a_1, over which the viscous gradients in the drop decay, controls the importance of the Couette contribution of the vapour flow. The Couette component does not contribute to the levitation of the drop; hence we find thinner films for decreasing shear stresses in the drop. For the case of infinitesimally small velocity gradient, i.e. no Marangoni flow, the model recovers that of Wachters[5] and Biance,[6] which will be used as a reference case, and the corresponding height of that case is called h_0.

The Marangoni flow thins the film as well, as shown in the right panel of Fig. 10, where the plate is set to $\Delta T = 50$ K. The thickness is compared with h_0 for various a_1. We find a strong decrease in film thickness for only a few Kelvin of temperature difference between the top and bottom of the drop. The viscous stresses from the drop still influence the Couette flow in the vapour gap as shown by the various curves. Our model predicts average vapour flow velocities of several tens of cm per second, in agreement with previous studies.[6,27] Significant influences of the Marangoni flow imply that U_p and U_c are of the same order. For the realistic values discussed earlier, $a_1 \approx 1$ and $a_2 \Delta T_{bt} \approx 25$, we find a reduction of h by a factor 2. Note that, for models using a no-shear boundary condition (i.e. $a_1 = \infty$), this would imply a change in plate superheat ΔT by a factor $2^4 = 16$.

The system can also be analysed from an energy based point of view. The vapour generation drives the flow and hence, work is performed. This kinetic energy is dissipated along the gap by
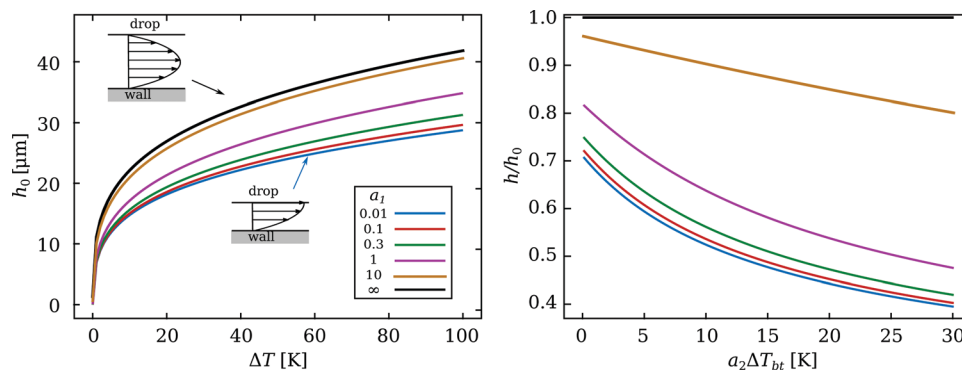

Fig. 10 Solutions of eqn (10) for an ethanol drop of $R = 1$ mm. The dissipation in the drop is varied via a_1. The black line corresponds to $U_c(a_1) = 0$: the limit of a no-shear-flow boundary condition,[5,6] whereas the blue curve approaches the limit of zero shear stress, see the flow sketches. The right panel shows the (scaled) thinning of the film, resulting from the Marangoni stress for various a_1, depending on the strength of the temperature gradient. Here, $\Delta T = 50$ K.

both the wall and the liquid drop,[46,47] where, for the latter, its strength scales with the viscosity and the length scale $(a_1/R)^2$. The Marangoni stress also performs work and thus acts as an energy source. The problem is then solved by adding the work originating from the vapour generation and the Marangoni stress and balance it with the viscous dissipation in the drop and the vapour gap due to the presence of the solid wall.

In our experiment, the Marangoni stress was changed by altering the box temperature. Addition of ethanol vapour in the box prior to the drop formation made it possible to form metastable Leidenfrost drops at plate temperatures even below the data shown in Fig. 8. The (temporarily) increase in vapour concentration in the box reduces the evaporation from the top of the drop and thus would suppress the Marangoni flow. Naturally, the evaporation rate and thus the cooling at the top of the drop decreases, leading to a thicker vapour layer. Therefore, the film becomes less subject to disturbances. The increase of the vapor concentration in the enclosure reduces the evaporation from the drop thus slowing down the evaporative cooling and, with it, the Marangoni flow. Two other factors tend to decrease the evaporation rate. In the first place, condensation at the walls acts as a vapour sink for temperatures below T_{sat} and this effect is reduced if the wall temperature is increased. Secondly, the warmer environment acts as a source of thermal energy besides the hot plate, which also tends to reduce evaporative cooling. The result is a thicker vapour film under the drop which is less sensitive to disturbances.

A reduction in the film thickness will also have an effect on the evaporation rate of the drop. The change in the (local) evaporation rate is also straightforward, since $\dot{m} \propto 1/h$, thus doubling for a decrease in vapour thickness by a factor 2. However, since the strength of the Marangoni stress is altered by influencing the evaporation rate at the top of the drop, it is far from trivial how these effects compare and determine the global drop evaporation rate.

6 Conclusions and outlook

We have shown experimentally that the Leidenfrost phenomenon and the corresponding Leidenfrost temperature T_L are influenced strongly by the environment. Increasing the ambient pressure increases T_L, which shows a linear relation with the saturation temperature of the liquid at the same environmental pressure. By non-dimensionalizing the temperatures by the ratio of latent and specific heat of the vapour, we show that all the liquids studied follow a universal curve, correlating the (non-dimensional) Leidenfrost temperature with the (non-dimensional) saturation temperature.

At ambient pressure we studied the existence of Leidenfrost drops at lower plate temperatures than T_L. These drops however are metastable: a drop which is carefully prepared in the Leidenfrost state, will not recover to it once a touchdown has (intentionally) occurred. We hypothesised that a minimal vapour thickness must form to prevent touch-down of (metastable) Leidenfrost drops: lowering the superheat leads to a thinner

vapour film. The temperature range at which metastable drops were observed depends strongly on the ambient temperature. T_L however does not depend on the ambient temperature and thus is not expected to appear in the non-dimensional prediction derived in Section 4. We explored the possibility that evaporation from the top of the drop leads to local cooling, and thus a Marangoni stress along the drop surface. Increasing the ambient temperature would reduce the strength of the Marangoni stress by suppressing the evaporation. This leads to a thinner vapour film for the same plate temperature.

We suggest that the resulting increase in vapour film thickness increases the stability of the metastable Leidenfrost drop. In this study we only provided a general concept, based on global estimates on the Leidenfrost dynamics. A follow-up studies aiming at solving the full transport problem numerically would yield quantitative insight on the proposed model, where the role of the ambient vapour concentration and temperature field in the box are of particular interest. Additional liquids should be assessed as well to investigate the potential universality of the phenomenon. Moreover, based on the study of these metastable Leidenfrost drops, we suggest that the Leidenfrost effect originates from the dynamics at the liquid–solid contact line, prior to levitation. A careful assessment of the contact line dynamics in the limit of non-wetting drops will provide more insight on this point, potentially leading to a full understanding of the Leidenfrost phenomenon. Further insight may be obtained by from studying binary and ternary Leidenfrost droplets, as volatilities and surface tension of the components bringing rich physicochemical hydrodynamics of the droplets[48] and offer the opportunity to make use of the relative initial concentration as an extra control parameter.[49]

Conflicts of interest

There are no conflicts to declare.

Acknowledgements

References

1 D. Quéré, *Annu. Rev. Fluid Mech.*, 2013, **45**, 197–215.
2 A. L. N. Moreira, A. S. Moita and M. R. Panão, *Prog. Energy Combust. Sci.*, 2010, **36**, 554–580.
3 D. Attinger, Z. Zhao and D. Poulikakos, *J. Heat Transfer*, 2000, **122**, 544–555.
4 J. Kim, *Int. J. Heat Fluid Flow*, 2007, **28**, 753–767.
5 L. H. J. Wachters, H. Bonne and H. J. van Nouhuis, *Chem. Eng. Sci.*, 1966, **21**, 923–936.

6 A.-L. Biance, C. Clanet and D. Quéré, *Phys. Fluids*, 2003, **15**, 1632–1637.

7 B. Sobac, A. Rednikov, S. Dorbolo and P. Colinet, *Phys. Rev. E: Stat., Nonlinear, Soft Matter Phys.*, 2014, **90**, 053011.

8 S. Chandra and C. T. Avedisian, *Proc. R. Soc. London, Ser. A*, 1991, **432**, 13–41.

9 T. Tran, H. J. J. Staat, A. Prosperetti, C. Sun and D. Lohse, *Phys. Rev. Lett.*, 2012, **108**, 036101.

10 M. Shirota, M. A. J. van Limbeek, C. Sun, A. Prosperetti and D. Lohse, *Phys. Rev. Lett.*, 2016, **116**, 064501.

11 C. Josserand and S. T. Thoroddsen, *Annu. Rev. Fluid Mech.*, 2016, **48**, 365–391.

12 M. A. J. van Limbeek, T. H. Nes and S. Vanapalli, *Int. J. Heat Mass Transfer*, 2020, **148**, 118999.

13 J. G. Leidenfrost, *De aquae communis nonnullis qualitatibus tractatus*, Ovenius, Duisburg, 1756.

14 H. Boerhaave, *Elementa Chemiae*, Lugduni Batavorum, 1732, pp. 258–259.

15 J. H. Snoeijer, P. Brunet and J. Eggers, *Phys. Rev. E: Stat., Nonlinear, Soft Matter Phys.*, 2009, **79**, 036307.

16 K. C. D. Hickman, *Ind. Eng. Chem.*, 1964, **56**, 18–31.

17 L. Maquet, B. Sobac, B. Darbois-Texier, A. Duchesne, M. Brandenbourger, A. Rednikov, P. Colinet and S. Dorbolo, *Phys. Rev. Fluids*, 2016, **1**, 053902.

18 M. A. J. Van Limbeek, B. Sobac, A. Rednikov, P. Colinet and J. H. Snoeijer, *J. Fluid Mech.*, 2019, **863**, 1157–1189.

19 K. J. Baumeister, R. C. Hendricks and T. D. Hamill, *Metastable Leidenfrost states*, National Aeronautics and Space Administration, 1966.

20 P. Bourrianne, C. Lv and D. Quéré, *Sci. Adv.*, 2019, **5**, eaaw0304.

21 K. J. Baumeister and F. F. Simon, *J. Heat Transfer*, 1973, **95**, 166–173.

22 H. Kim, B. Truong, J. Buongiorno and L.-W. Hu, *Appl. Phys. Lett.*, 2011, **98**, 083121.

23 H.-m. Kwon, J. C. Bird and K. K. Varanasi, *Appl. Phys. Lett.*, 2013, **103**, 201601.

24 J. D. Bernardin and I. Mudawar, *J. Heat Transfer*, 1999, **121**, 894–903.

25 M. A. J. van Limbeek, M. Shirota, P. Sleutel, C. Sun, A. Prosperetti and D. Lohse, *Int. J. Heat Mass Transfer*, 2016, **97**, 101–109.

26 M. Khavari and T. Tran, *Phys. Rev. E*, 2017, **96**, 043102.

27 M. A. J. van Limbeek, M. H. Klein Schaarsberg, B. Sobac, A. Rednikov, C. Sun, P. Colinet and D. Lohse, *J. Fluid Mech.*, 2017, **827**, 614–639.

28 D. Orejon, K. Sefiane and Y. Takata, *Phys. Rev. E: Stat., Nonlinear, Soft Matter Phys.*, 2014, **90**, 053012.

29 G. Emmerson, *Int. J. Heat Mass Transfer*, 1975, **18**, 381–386.

30 G. S. Emmerson and C. W. Snoek, *Int. J. Heat Mass Transfer*, 1978, **21**, 1081–1086.

31 W. Bouwhuis, K. G. Winkels, I. R. Peters, P. Brunet, D. van der Meer and J. H. Snoeijer, *Phys. Rev. E: Stat., Nonlinear, Soft Matter Phys.*, 2013, **88**, 023017.

32 Q. Cui, S. Chandra and S. McCahan, *J. Heat Transfer*, 2001, **123**, 719–728.

33 H. Linke, B. J. Alemán, L. D. Melling, M. J. Taormina, M. J. Francis, C. C. Dow-Hygelund, V. Narayanan, R. P. Taylor and A. Stout, *Phys. Rev. Lett.*, 2006, **96**, 154502.

34 G. Lagubeau, M. Le Merrer, C. Clanet and D. Quéré, *Nat. Phys.*, 2011, **7**, 395–398.

35 P. Yi, P. Thurgood, N. Nguyen, H. Abdelwahab, P. Petersen, C. Gilliam, K. Ghorbani, E. Pirogova, S.-Y. Tang and K. Khoshmanesh, *Soft Matter*, 2020, **16**, 8854–8860.

36 A. A. Mills and J. D. Fry, *Eur. J. Phys.*, 1982, **3**, 152.

37 A. Mills and N. Sharrock, *Eur. J. Phys.*, 1986, **7**, 52.

38 K. Kroenlein, *et. al.*, NIST/TRC Web Thermo Tables (WTT), NIST SRSD-3, Version 2-2012-1-pro technical report.

39 L. R. Villegas, R. Alis, M. Lepilliez and S. Tanguy, *J. Comput. Phys.*, 2016, **316**, 789–813.

40 J. M. Kolinski, L. Mahadevan and S. Rubinstein, *EPL*, 2014, **108**, 24001.

41 S. Lyu, V. Mathai, Y. Wang, B. Sobac, P. Colinet, D. Lohse and C. Sun, *Sci. Adv.*, 2019, **5**, eaav8081.

42 D. V. Zaitsev, D. P. Kirichenko, V. S. Ajaev and O. A. Kabov, *Int. Heat Transfer Conf. Digital Library*, 2018.

43 A. Shahriari, P. V. Acharya and V. Bahadur, ASME 2018 16th Int. Conf. on Nanochannels, Microchannels, and Minichannels, 2018, p. V001T06A006.

44 A. Bouillant, T. Mouterde, P. Bourrianne, A. Lagarde, C. Clanet and D. Quéré, *Nat. Phys.*, 2018, **14**, 1188–1192.

45 V. S. Ajaev and O. A. Kabov, *Int. J. Heat Mass Transfer*, 2017, **108**, 918–932.

46 S. Wildeman, C. W. Visser, C. Sun and D. Lohse, *J. Fluid Mech.*, 2016, **805**, 636–655.

47 O. Ramrez-Soto, V. Sanjay, D. Lohse, J. T. Pham and D. Vollmer, *Sci. Adv.*, 2020, **6**, eaba4330.

48 D. Lohse and X. Zhang, *Nat. Rev. Phys.*, 2020, 1–18.

49 S. Lyu, H. Tan, Y. Wakata, X. Yang, C. K. Law, D. Lohse and C. Sun, *Proc. Natl. Acad. Sci. U. S. A.*, 2021, **118**, e2016107118.